Numerical and experimental investigation of heat transfer across a nanoscale gap between a magnetic recording head and various media

S. Sakhalkar,[1, a)] Q. Cheng,[1] A. Ghafari,[1] Y. Ma,[2] and D. Bogy[1]
[1)] *University of California at Berkeley, Berkeley, California 94720, USA*
[2)] *Texas A&M University, College Station, Texas 77843, USA*

(Dated: 25 November 2019)

With the emergence of Heat-Assisted Magnetic Recording and Microwave-Assisted Magnetic Recording, understanding nanoscale heat transfer at the head-media interface is crucial for developing reliable hard disk drives. There is a need to develop a methodology that uses a spacing-dependent nanoscale heat transfer coefficient, determined by using wave-based radiation and van der Waals forces driven phonon conduction theories to predict head temperatures in hard disk drives. We present a numerical model to simulate the head temperature due to heat transfer across a closing nanoscale gap between the head and the media (non-rotating) and compare our results with static touchdown experiments performed with a head resting on three different media (Si, magnetic disks with AlMg and glass substrates). The Thermal Fly-Height Control (TFC) heater in the head is powered to create a local protrusion, leading to contact of a resistive Embedded Contact Sensor (ECS) that is used to measure the temperature change. As the ECS approaches the media, enhanced phonon conduction heat transfer causes a drop in the ECS temperature vs TFC power curve. Our model shows that the introduction of van der Waals forces between the head and the media during computation of the head's thermal protrusion causes a steeper drop in the simulated ECS temperature curve, ensuring a good quantitative match with experiments for all of the media materials tested and different initial ECS-media spacings. We isolate the effect of air conduction on ECS cooling by comparing our simulations with experiments performed in air vs vacuum.

Technologies such as Heat-Assisted Magnetic Recording (HAMR) and Microwave-Assisted Magnetic Recording (MAMR) are under rapid development to achieve storage densities beyond 1 Tb/in^2 in hard disk drives (HDDs)[1,2]. However, head overheating is a major reliability issue that needs to be addressed for both of these technologies. During HAMR writing, a complex laser delivery system integrated into the head is used to create a local hot spot on the disk, generating high temperatures on the disk ($\sim$500 ^{o}C) and the head ($\sim$300 ^{o}C). This can cause mass transfer in the head-disk interface (HDI), creating further reliability issues[3–6]. The high current density in the Spin Torque Oscillator in MAMR heads ($\sim 10^8$ A/cm^2) also causes high head temperatures (>200 ^{o}C)[7]. Moreover, with the minimum fly height of less than 10 nm in contemporary HDDs, classical heat transfer theory can no longer be used to predict temperatures in the head and the disk. Previous experimental studies[8,9] and wave-based theories of radiation and phonon conduction (or tunneling)[10–15] have shown that heat flux increases significantly at nanoscale gaps. Several other theoretical studies also predict high heat flux between two surfaces separated by a small gap[16–19]. There is a need to develop a methodology that uses theoretical curves for spacing-dependent nanoscale heat transfer coefficients to predict head/media temperatures in actual HDDs.

Ma et al. developed a setup (static touchdown experiment) to study heat flux across a gap between two stationary bodies as the spacing between them closes in a controlled manner from tens of nm to contact[20]. In this experiment, the crown feature of the head Air Bearing Surface (ABS) is used to control the initial spacing between the head and the media (non-rotating)[20,21] (Fig. 1). After loading the head onto the media, the initial spacing between the trailing edge body of the head and the media can be adjusted via a rocking motion about the center caused by moving the media forward or backward. With an initial spacing of 10-50 nm, the Thermal Fly Height Control (TFC) heater in the head is powered to generate a local thermal protrusion near the trailing edge, causing touchdown. A near-surface resistive temperature sensor (Embedded Contact Sensor or ECS) is used to measure the temperature change at the head surface due to the heat flux across the gap. The TFC Power is kept on for a long enough duration in the experiment to ensure that the measured ECS temperature has reached steady state. This entire setup is placed inside a chamber, which can reach high vacuum (< 1e-4 Torr).

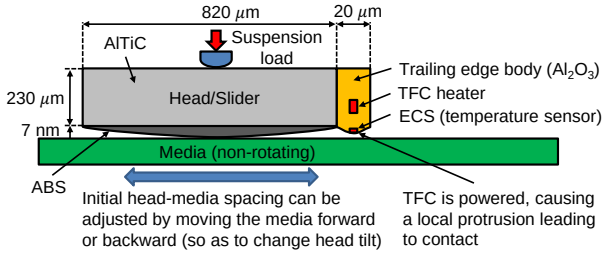

FIG. 1. Static touchdown experiment schematic (side view)

Several studies have demonstrated that the ECS is an effective tool in understanding heat transfer in the HDI[22–25]. Using the static touchdown experiment, Ma et al. observed that enhanced heat transfer at the HDI causes a drop in the ECS temperature as the ECS approaches the media[20]. They also observed a hysteresis loop during load-unload experiments, suggesting that van der Waals (vdW) forces play an important role on HDI heat transfer[20]. Subsequently, Ma et al. performed phonon conduction-based simulation of ECS cooling during static touchdown, however, their model shows qualitative, but

[a)] Electronic mail: siddhesh_sakhalkar@berkeley.edu.

not good quantitative agreement with experiments[21,26]. Moreover, vdW forces were not considered while determining the thermal protrusion of the head in these numerical studies.

In this study, we present a numerical model to simulate the head temperature profile during static touchdown and compare our results with experiments performed with a head on different media (Si wafer, magnetic disks with AlMg/glass substrate). We first discuss the heat transfer coefficient between two half-spaces based on a wave-based phonon conduction theory as a function of the spacing, the temperatures and material properties of both half-spaces. Next, the numerical model that uses this heat transfer coefficient to simulate head temperature is presented. Simulated ECS temperature during static touchdown with different initial ECS-media spacings, in different environments (air vs vacuum) and on the three different media are compared with corresponding experiments. This is followed by a discussion and conclusion.

During static touchdown of the head on the disk, three major heat transfer schemes exist: air conduction, phonon conduction and radiation. The heat transfer coefficient for air conduction (htc_{air}) can be obtained using the temperature jump theory and the modified mean free path of air due to boundary scattering[27,28]. Intermolecular vdW forces between two half-spaces ($\nu = A, B$) with temperatures T_A, T_B and spacing h cause phonons to transfer energy from one half-space to the other (phonon conduction). When the system of the two half-spaces is in equilibrium (no heat flux), phonon waves in both half-spaces are described by the Bose-Einstein distribution (or Planck function), $p^2(\omega,T)|_{equil} = (\exp(\frac{\hbar\omega}{k_B T}) - 1)^{-1}$, which is a function of the equilibrium temperature ($T_A = T_B = T$) and frequency[15]. When the system is in a non-equilibrium condition (steady state heat flux), the distribution function of phonons in each half-space ν is a modified version of Bose-Einstein distribution (modified Planck function)[15] and is given by $(p_\nu^\pm)^2(\omega,T_\nu,\mu_\nu) = (\exp(\frac{\hbar\omega[1\mp\mu_\nu]}{k_B T_\nu}) - 1)^{-1}$. Here μ_ν is an unknown factor in $(0,1)$ indicating how much the system has deviated from equilibrium ($\mu_\nu = 0$) and $\pm$ represent waves travelling in the positive (away from half-space) and negative (into the half-space) directions respectively. $(p_\nu^\pm)^2$ is displaced from the equilibrium distribution, $p^2(\omega,T)|_{equil}$, by a term $\hbar\mu_\nu\omega$, which can be interpreted physically as the chemical potential[29]. The displacement term, $\hbar\mu_\nu\omega$ is proportional to the phonon momentum and goes to zero as $\omega \to 0$. We note that since $0 < \mu_\nu < 1$, $(p_\nu^\pm)^2$ is always positive. The resultant heat flux $Q(T_A,T_B,h)$ between the two half-spaces is given by two different representations[13,14]

$$Q = N\int_\Omega \left\{(p_\nu^+)^2 - (p_\nu^-)^2\right\}\frac{\hbar\omega^3}{8\pi^2 c_\nu^2}\sin(2\theta_\nu)d\theta_\nu d\omega, \quad \nu = A,B, \tag{1}$$

where $N = 3$ is the number of polarizations, ω, θ_ν are the wave frequency and angle of propagation, ρ_ν, c_ν are the material density and wave speed. The domain of integration $\Omega = \Omega(\omega,\theta_\nu)$ determines the wave vectors that contribute to Q and is determined using the compatibility conditions in Ref. 14. The effect of vdW forces on Q is considered through the reflection coefficient, R. When phonons are considered as propagating waves inside a medium, the energy transfer between layers is quantified according to the reflection coefficient of waves on the interface. For the energy transfer between two layers separated by vacuum, R depends on the vdW forces between the two layers. A detailed derivation for the expression of $R(\omega,\theta_\nu,h;\rho_\nu,c_\nu)$ using vdW forces can be found in Ref. 11. R affects the domain of integration, Ω in Eq. (1) and thus determines how much energy can be transferred between the two half-spaces due to vdW forces.[14] Apart from R, Ω also depends on $p_\nu^\pm$, the critical angle (a function of c_ν)[11,14] and Debye frequency of A, B.[14]

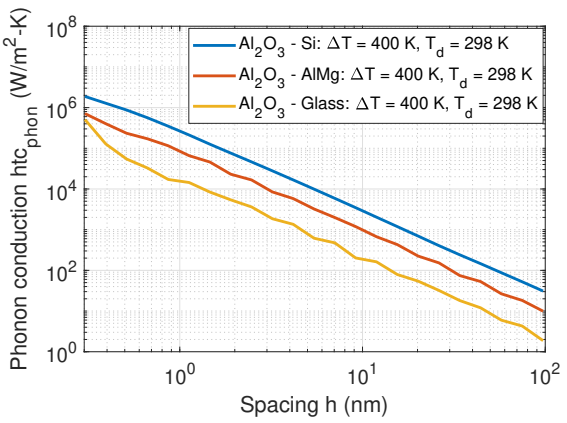

FIG. 2. Phonon conduction heat transfer coefficient, htc_{phon} vs spacing, h at T_d = 298 K and ΔT = 400 K for three different media

We have two equations from (1) and 3 unknowns (μ_A,μ_B,Q), resulting in a range of possible solutions for Q. By using the Maximum Entropy Production Principle (MEPP)[30], we choose the maximum Q as the solution[14]. Using this methodology, the phonon conduction heat transfer coefficient ($htc_{phon} = \frac{Q(T_s,T_d,h)}{T_s - T_d}$) is determined as a function of the disk temperature T_d, the slider-disk temperature difference $\Delta T = T_s - T_d$ and the spacing h. We plot htc_{phon} vs h for three media materials: Si, AlMg, glass in Fig. 2. The slider material is assumed to be Al_2O_3. Our results suggest that htc_{phon} can be approximated using the following equation (0.1 nm $< h <$ 100 nm, 4 K $< \Delta T <$ 400 K, 298 K $< T_d <$ 398 K)

$$ln(htc_{phon}) = c_1 ln(h) + c_2 ln\left(\frac{\Delta T}{400}\right) + c_3 ln\left(\frac{T_d}{298}\right) + b \tag{2}$$

Parameters c_1, c_2, c_3, b depend on the density (ρ_ν), wave speed (c_ν) and Debye frequency of both half-spaces (Table I). While ρ_ν and c_ν affect phonon conduction, the decreasing trend in htc_{phon} for Si, AlMg, glass can largely be explained by a decreasing trend in Debye temperatures (645 K, 464 K, 290 K respectively). A larger Debye temperature or frequency implies a larger range of allowable frequencies of phonon waves in Ω, leading to a larger Q. At nanoscale spacings, the heat transfer coefficient due to radiation ($\sim 10^3$ W/m^2·K)[12] is much smaller than that due to phonon conduction ($\sim 10^6$ W/m^2·K), hence radiation is ignored in this study.

As $h \to 0$, the net heat transfer coefficient due to phonon

TABLE I. Phonon conduction parameters for three different media

Material	c_1	c_2	c_3	b
Si	-1.93	-0.83	1.4	12.33
Al-Mg	-1.97	-0.86	1.65	11.34
Glass	-2.11	-0.89	0.5	10.10

and air conduction, $htc_{total}(T_s, T_d, h) = htc_{phon} + htc_{air}$ increases (Eq. (2)). In reality, htc_{total} would be limited by the interface thermal conductance when the head and the media come into contact. For most phonon mediated interfaces, the interface thermal conductance lies in the range: 2e7 to 2e8 W/m^2·K.[31] Hence, we limit htc_{total} to a constant interface thermal conductance: 5e7 W/m^2·K for head-Si interface and 3e7 W/m^2·K for head-AlMg disk, head-glass disk interfaces.

The net heat transfer coefficient due to phonon and air conduction, $htc_{total}(T_s, T_d, h)$ is integrated into a finite element ANSYS model of the slider and the disk. The bulk of the slider block (820 μm x 700 μm x 230 μm) is made of AlTiC (k = 20 W/m·K)[32], while the trailing edge (TE) portion (20 μm x 700 μm x 230 μm) is made of Al_2O_3 (k = 1.8 W/m·K)[32] (Fig. 1). Additionally, the TE body has several metal components (such as the reader, writer and shields), which are much better thermal conductors than Al_2O_3 and affect the heat diffusion inside the head. The focus of this study is to understand the heat transfer in the HDI and model its effect on the ECS temperature. To avoid an overly complex geometric model, we define an effective thermal conductivity (k_{eff}) and effective thermal expansion coefficient (α_{eff}) for the part of the TE body near the ABS that contains these metal elements (20 μm x 40 μm x 30 μm). Using the values k_{eff} = 50 W/m·K and α_{eff} = 7e-6 K^{-1}, the initial slope of the ECS temperature vs TFC Power curve during the static touchdown simulation on Si wafer in air (0.85 °C/mW) agrees with the measured slope during the experiment (Fig. 3). We note that the value of k_{eff} is dependent on the head design and lies within the range of thermal conductivity (W/m·K) of all the components in the head: 35 for NiFe (reader/shield), 403 for Cu (writer), 1.8 for Al_2O_3[32]. We create a local disk model (1150 μm x 800 μm x 330 μm) and enforce all boundary faces (except the face opposite to ABS) at room temperature (25 °C).

The slider temperature profile (T_s) during the static touchdown simulation is determined using a steady state thermal conduction simulation with a heat source (TFC), metal suspension cooling (2000 W/m^2·K)[33] on the back surface and $htc_{total}(T_s, T_d, h)$ on the ABS. The disk temperature profile (T_d) is determined using a steady state thermal conduction simulation with the same $htc_{total}(T_s, T_d, h)$ on the surface opposite to the ABS. The head-disk spacing (h) is determined using a linear elasto-static simulation with specified temperature profile (T_s) and vdW force on the ABS to evaluate the head's TFC heating-induced protrusion. The net vdW force between each ABS element (Δ) and the disk is given by[34]

$$F_{vdW} = \frac{A}{6\pi}\iint_{\Delta}\frac{dxdy}{h^3} - \frac{B}{45\pi}\iint_{\Delta}\frac{dxdy}{h^9} \qquad (3)$$

We assume that A = 0.4e-19 J, B = 1e-76 Jm^6. The resultant

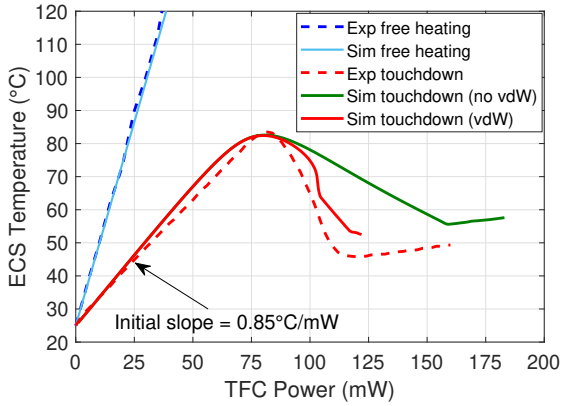

FIG. 3. Static touchdown experiment and simulation on Si in air with initial spacing of 21.3 nm. Solid green curve excludes vdW forces while computing slider's thermal protrusion, while solid red curve considers vdW forces while computing slider's thermal protrusion.

non-linear problem for T_s, T_d and h (or equivalently htc_{total}) is solved using Broyden's (Quasi-Newton) method[35].

We note that our model considers the effect of vdW forces in two different ways. Firstly, the effect of vdW forces is considered on the phonon conduction heat flux Q in Eq. (1) thorugh the reflection coefficient. Secondly, we also consider the effect of vdW forces while determining the thermal protrusion of the slider through Eq. (3).

Fig. 3 shows the ECS temperature vs TFC power during free heating of the slider in air (with no media present). During free heating, there is negligible cooling on the ABS and the metal suspension back cooling is poor compared to static touchdown, since the suspension is not loaded. With a low back cooling coefficient for free heating (1200 W/m^2·K vs 2000 W/m^2·K for static touchdown[33]), the simulated free heating ECS temperature curve agrees with the experiment.

Fig. 3 also plots the simulated ECS temperature vs TFC power for static touchdown of the head on Si in air with an initial ECS-media spacing of 21.3 nm. We consider two cases: (a) vdW forces are not considered while determining the thermal protrusion of the slider (solid green curve in Fig. 3), (b) vdW forces are considered while determining the slider's thermal protrusion using Eq. (3) (solid red curve). Both simulation cases consider the effect of vdW forces on Q through the reflection coefficient in Eq. (1). For both cases, as the TFC power is increased, initially, the ECS temperature increases due to TFC heating. However, when the ECS-media spacing becomes smaller than about 2 nm, enhanced phonon conduction heat transfer causes a drop in the ECS temperature.

The simulation without vdW forces (solid green curve in Fig. 3) shows a much more gradual drop in the ECS temperature than that in the experiment (dashed red curve). As the ECS approaches touchdown, enhanced phonon conduction causes cooling and impedes touchdown. On the other hand, attractive vdW forces between the slider and the media accelerate the touchdown process. Hence, the simulation with vdW forces (solid red curve) shows a steeper drop in the ECS

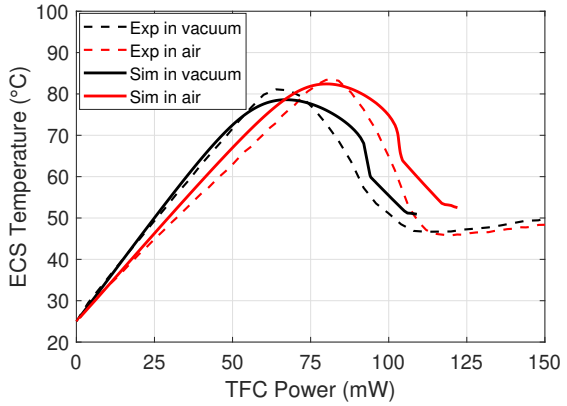

FIG. 4. Static touchdown simulation on Si in air (htc_{air} included) and in vacuum (htc_{air} excluded) and comparison with experiment in air and in vacuum. Initial spacing is 21.3 nm; vdW forces are included.

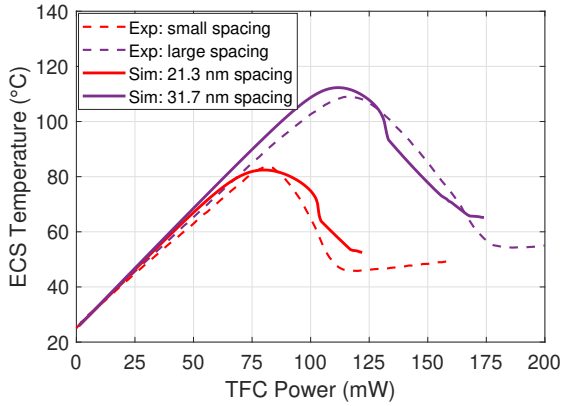

FIG. 5. Static touchdown simulation on Si in air with initial spacing of 21.3 nm, 31.7 nm (with vdW) and comparison with two experiments performed at different initial spacings in air. Since we do not know the initial spacing in the experiment, we choose the initial spacing in the simulation to ensure a good fit with the experiment.

temperature curve than the simulation without vdW forces and agrees much better with the experiment. See supplementary material Fig. S1 for plot of htc_{total} vs TFC Power for the simulations with and without vdW forces.

To isolate the effect of air conduction on ECS cooling, we performed touchdown experiments in vacuum and compared the simulation with and without air conduction (including vdW forces) with the experiment in air and in vacuum (Fig. 4). When we include air conduction in the model, htc_{total} increases during the initial TFC heating zone (0-66 mW). This causes the ECS temperature to drop, which explains why the red curve is below the black curve from 0 to 66 mW. A lower ECS temperature causes a smaller TFC protrusion, leading to a larger spacing and hence a smaller htc_{phon} for the simulation with air as compared to that without air. Hence the ECS temperature is lower for simulation without air (black curve)

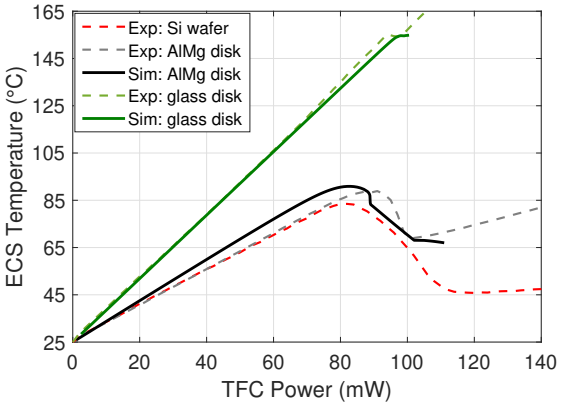

FIG. 6. Effect of media material (Si wafer vs AlMg disk vs glass disk) on head cooling during static touchdown experiment in air.

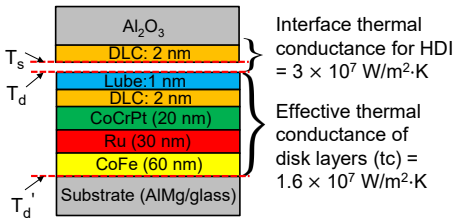

FIG. 7. PMR disk multi-layered structure.

than that with air (red curve) for TFC power $>$ 66 mW (when phonon conduction dominates). The shift in the ECS curve with/without air conduction agrees well with the shift in the experiment in air vs vacuum. Since the media is stationary in this experiment, air conduction has a small effect on the ECS temperature (as opposed to the flying case over a rotating disk, where air cooling would have a more significant impact).

As the initial ECS-media spacing is increased in the experiment, the peak ECS temperature increases and the peak is attained at a higher TFC power (Fig. 5). The same trend is observed in the simulated ECS temperature curve, as the initial spacing is increased from 21.3 nm to 31.7 nm. Moreover, for both initial spacings, we use the same value of A, B in Eq. (3). A good quantitative match between the experiment and simulation for both spacings strongly suggests that vdW force is responsible for the steep drop in the ECS cooling curve.

To study the effect of media on ECS cooling, we performed touchdown experiments on Perpendicular Magnetic Recording (PMR) disks with AlMg and glass substrates and compared the results with the touchdown curve on Si (Fig. 6). PMR disks have a multi-layered structure (Fig. 7) comprising of lube, DLC (diamond-like-carbon), magnetic layers (CoCrPt, Ru, CoFe) and the substrate (AlMg or glass). Since the characteristic dimension along the surface ($\sim \mu$m) is much larger than the height of the disk layers ($\sim$nm), we model the effect of the layers by computing an "effective thermal con-

ductance" (tc) of the layered structure, which is defined as

$$\frac{1}{tc} = \Sigma_i \left(\frac{L_i}{k_i} + \frac{1}{h_i} \right) \quad ; \quad k_i(L_i) = \frac{k_{i,bulk}}{1 + \frac{4\Lambda_{bulk}}{3L_i}} \tag{4}$$

$$Q_{total} = htc_{total}(T_s - T_d) = tc(T_d - T_d') \tag{5}$$

Here L_i is the thickness of the i^{th} layer, k_i is the thin-film thermal conductivity of the layer material, h_i is the interface thermal conductance between layers i, $i+1$. The temperature difference between the top surfaces of the disk (T_d) and the AlMg substrate (T_d') is determined using Eq. (5). We assume h_i = 4e9 W/m^2·K for metal-metal interfaces[36] and h_i = 1e8 W/m^2·K for metal-dielectric interfaces[31]. The reduced thermal conductivity of each magnetic layer $k_i(L_i)$ due to boundary scattering is determined using Matthiessen's rule[37] in Eq. (4) (we assume bulk mean free path of electrons, Λ_{bulk} in the magnetic layer is 40 nm). The bulk thermal conductivity of the magnetic layer materials, $k_{i,bulk}$ can be found in Ref. 38. k_i of DLC is 1 W/m·K and that of the lube is 0.07 W/m·K.[3,39] With these assumptions, tc for the AlMg disk layers is computed as 1.6e7 W/m^2·K. The interface thermal conductance for the HDI is expected to be sensitive to the disk roughness and is assumed to be 3e7 W/m^2·K. This value is chosen such that the touchdown simulation on the AlMg disk in air with vdW and initial spacing of 24 nm (solid black curve) agrees with the experiment (dashed grey curve). Using the same layered structure, we simulate the touchdown curve for the glass disk in air with vdW and initial spacing of 41 nm (solid green curve), which also agrees well with the experiment (dashed green curve). See supplementary material Fig. S2 for comparison of htc_{total} vs TFC Power for Si, Al-Mg disk and glass disk.

If the media is a good thermal conductor, it is able to effectively diffuse the heat transferred from the head, leading to stronger cooling of the ECS. Glass has a much lower thermal conductivity (0.9 W/m·K) than Si (148 W/m·K) and hence shows a much smaller drop in the touchdown curve. AlMg has a comparable thermal conductivity (117 W/m·K)[40] to Si, yet shows a smaller drop in the touchdown curve than Si. The layers on top of the AlMg substrate (tc = 1.6e7 W/m^2·K) make the AlMg disk an overall poor conductor (compared to Si). The presence of the disk layers, along with lower thermal conductance for the HDI (3e7 W/m^2·K for head-AlMg disk vs 5e7 W/m^2·K for head-Si, which is possibly caused by larger RMS surface roughness of the AlMg disk: S_q = 0.2 nm than that of Si: S_q = 0.1 nm), account for the smaller drop in the simulated touchdown curve on AlMg disk compared to Si.

In conclusion, we have developed a numerical model to simulate the head temperature profile during static touchdown and compared our results with experiments performed with a head on three different media (Si, AlMg disk, glass disk). As the ECS approaches touchdown with increasing TFC power, enhanced phonon conduction causes a drop in the ECS temperature vs TFC power curve. Our model shows that the introduction of vdW forces between the head and the media during computation of the head's thermal protrusion causes a steeper drop in the ECS temperature curve and ensures a good quantitative match with experiments for all of the media materials tested, different initial ECS-media spacings and in different environments (air vs vacuum).

See the supplementary material for plots of htc_{total} vs TFC Power with and without vdW forces and for different media (Si, AlMg disk, glass disk).

This project was supported by the Computer Mechanics Laboratory at UC Berkeley. We thank JP Peng, Robert Smith of WD for supplying components and helpful discussions.

[1] M. H. Kryder, E. C. Gage, T. W. McDaniel, W. A. Challener, R. E. Rottmayer, G. Ju, Y.-T. Hsia, and M. F. Erden, Proc. IEEE **96**, 1810 (2008).
[2] J.-G. Zhu, X. Zhu, and Y. Tang, IEEE Trans. Magn. **44**, 125 (2008).
[3] J. Kiely, P. Jones, Y. Yang, J. Brand, M. Anaya-Dufresne, P. Fletcher, F. Zavaliche, Y. Toivola, J. Duda, and M. Johnson, IEEE Trans. Magn. **53**, 3300307 (2017).
[4] S. Sakhalkar and D. Bogy, Tribol. Lett. **65**, 166 (2017).
[5] S. Sakhalkar and D. Bogy, Tribol. Lett. **66**, 145 (2018).
[6] S. Sakhalkar and D. Bogy, IEEE Trans. Magn. **55**, 3300506 (2019).
[7] C. Boone, J. Li, I. Nunokawa, E. Schreck, M. Sugiyama, I. Tagawa, and Y. Udo, *US Patent 8995088B1 (31 March 2015)*.
[8] S. Shen, A. Narayanaswamy, and G. Chen, Nano Lett. **9**, 2909 (2009).
[9] K. Kim, B. Song, V. Fernndez-Hurtado, W. Lee, W. Jeong, L. Cui, D. Thompson, J. Feist, M. T. H. Reid, F. J. Garca-Vidal, J. C. Cuevas, E. Meyhofer, and P. Reddy, Nature **528**, 387 (2015).
[10] B. Budaev and D. Bogy, Appl. Phys. Lett. **104**, 061109 (2014).
[11] B. Budaev and D. Bogy, J. Appl. Phys. **117**, 104512 (2015).
[12] B. Budaev, A. Ghafari, and D. Bogy, J. Appl. Phys. **119**, 144501 (2016).
[13] B. Budaev and D. Bogy, Appl. Phys. Lett. **109**, 231905 (2016).
[14] B. Budaev and D. Bogy, Proc. R. Soc. A **473**, 20160584 (2017).
[15] B. Budaev and D. Bogy, Z. Angew. Math. Phys. **69**, 71 (2018).
[16] R. Prasher, Appl. Phys. Lett. **94**, 041905 (2009).
[17] M. Prunnila and J. Meltaus, Phys. Rev. Lett. **105**, 125501 (2010).
[18] Y. Ezzahri and K. Joulain, Phys. Rev. B **90**, 115433 (2014).
[19] C. Henkel and P. P. Schmidt, J. Opt. Soc. Am. B **36**, C10 (2019).
[20] Y. Ma, A. Ghafari, B. Budaev, and D. Bogy, Appl. Phys. Lett. **108**, 213105 (2016).
[21] Y. Ma, A. Ghafari, B. Budaev, and D. Bogy, IEEE Trans. Magn. **53**, 3300105 (2017).
[22] H. Wu and D. Bogy, Appl. Phys. Lett. **110**, 033104 (2017).
[23] J. Zheng, Y.-K. Chen, and Q. Zhou, Sci. Rep. **8**, 3343 (2018).
[24] N. Zuckerman, J. D. Kiely, M. C. Anaya-Dufresne, M. T. Johnson, and R. M. Crone, IEEE Trans. Magn. **55**, 3300205 (2019).
[25] Y. Ma, S. Xue, J.-P. Peng, and D. B. Bogy, IEEE Trans. Magn. **51**, 3300504 (2015).
[26] Y. Ma, A. Ghafari, Y. Wu, and D. Bogy, "A study of the nanoscale heat transfer in the hdd head-disk interface based on a static touchdown experiment," IEEE Trans. Magn. (unpublished).
[27] S. Zhang and D. Bogy, Int. J. Heat Mass Transf. **42**, 1791 (1999).
[28] D. Chen, N. Liu, and D. Bogy, J. Appl. Phys. **105**, 084303 (2009).
[29] P. Wurfel, J. Phys. C: Solid State Phys. **15**, 3967 (1982).
[30] L. M. Martyushev and V. D. Seleznev, Phys. Rep. **426**, 1 (2006).
[31] D. G. Cahill, K. Goodson, and A. Majumdar, ASME J. Heat Transfer **124**, 223 (2001).
[32] M. Kurita, J. Xu, M. Tokuyama, K. Nakamoto, S. Saegusa, and Y. Maruyama, IEEE Trans. Magn. **41**, 3007 (2005).
[33] J. Dahl and D. B. Bogy, Tribol Lett. **54**, 35 (2014).
[34] L. Wu and D. B. Bogy, ASME J. Tribol. **124**, 562 (2002).
[35] C. G. Broyden, Math. Comput. **19**, 577 (1965).
[36] B. C. Gundrum, D. G. Cahill, and R. S. Averback, Phys. Rev. B **72**, 245426 (2005).
[37] L. Jiji, "Heat conduction," (Springer, Berlin, Heidelberg, 2009) Chap. 11, pp. 347–401, 3rd ed.
[38] A. Ovcharenko, M. Yang, K. Chun, and F. E. Talke, IEEE Trans. Magn. **46**, 770 (2010).
[39] M. Shamsa, W. L. Liu, A. A. Balandin, C. Casiraghi, W. I. Milne, and A. C. Ferrari, Appl. Phys. Lett. **89**, 161921 (2006).
[40] M. Suk, P. Dennig, and D. Gillis, ASME J. Tribol. **122**, 264 (1999).